PAPER

Check for updates

Closed-shell d^{10}–d^{10} in [AuCl(CNR)]$_n$ and [AuCl(CO)]$_n$ (n = 1, 2; R = −H, −CH$_3$, −Cy) complexes: quantum chemistry study of their electronic and optical properties

Fernando Mendizabal [iD] *[a] and Sebastián Miranda-Rojas *[b]

The electronic structure and spectroscopic properties of [AuCl(CNR)] and [AuCl(CO)] (R = −H, −CH$_3$, −Cy) complexes with d^{10}–d^{10} type interactions were studied at the post-Hartree–Fock (MP2, SCS-MP2, CCSD(T)) and density functional theory levels. It was found that the nature of the intermetal interactions is consistent with the presence of an electrostatic (dipole–dipole) contribution and a dispersion-type interaction. The absorption spectra of these complexes were calculated using the single excitation time-dependent (TD) method at the DFT and SCS-CC2 levels. The calculated values are in agreement with the experimental range, where the absorption and emission energies reproduce the experimental trends, with large Stokes shifts. According to this, intermetallic interactions were found to be mainly responsible for the metal–metal charge transfer (MMCT) electronic transitions among the models studied.

1. Introduction

Systems chemistry is a new area in the description of the unique properties of compounds.[1–3] These systems, constructed from the interactions of different components, generate properties that cannot emerge from the system's components acting in isolation,[4,5] and are applicable to new fields such as materials science, supramolecular chemistry, and nanochemistry. Moreover, with the aid of modeling, computational, and theoretical tools, understanding of the behavior of systems chemistry is constantly improving, which will allow the rational design of new materials with modulable properties.[6] At the simplest level, noncovalent interactions (NCIs) among molecules can lead to the emergence of large structures as a result of self-assembly processes and supramolecular chemistry.[7–9]

Within this broad field, we are interested in evaluating the ability of heavy metals, such as gold, in the formation of stable self-assembly and inorganic complexes with optical properties,[10–12] aiming to provide new insights into the relationship between structure and optical response. The understanding of these systems comes from the calculation of their intermolecular interactions energies and determining how these lead to structures and patterns that result in the target optical properties; thus, allowing the relationship

between structure and optical properties to be rationalized.[13–17] A central point of the analysis described above is that an in-depth understanding of the relationship between structure and the luminescent metal-based optical response from materials will contribute towards the optimization of their properties.[11,18,19] In this context, the observation of absorption/luminescence has been tied to the presence of close Au–Au attractions in solid and solvent states.[20,21] Such gold complexes have provided the opportunity to understand the excited states in broad emission color coverage.[11] Supramolecular chemistry systems control of functional metal complexes plays an essential role in determining charge transport and optical properties.[22]

Metal–metal interactions are known as metallophilic interactions, and when referring to gold atoms in particular, are defined as "aurophilic interactions".[12,13] These closed-shell interactions are estimated to be energetically similar to hydrogen bonds (20–50 kJ mol^{-1}) in the case of gold(I) and to be weaker for metals such as silver(I), copper(I), platinum(II) and other metals.[23–25] Metallophilic interactions have been determined experimentally *via* solid-state X-ray diffraction[26–29] and nuclear magnetic resonance (NMR)/absorption/emission/ Raman spectroscopic measurements.[30,31] From a theoretical point of view, metallophilic interactions have been understood as being a contribution of two terms to the equilibrium distance: dispersion and ionic.[32–44] Relativistic effects contribute between 20% and 30% to the energy of interactions[14] for heavy atoms. In recent years, researchers have proposed that the nature of metallophilic interactions is represented by strong Pauli repulsion at close range, which is

[a]Departamento de Química, Facultad de Ciencias, Universidad de Chile, Casilla 653, Santiago, Chile. E-mail: hagua@uchile.cl

[b]Departamento de Ciencias Químicas, Facultad de Ciencias Exactas, Universidad Andres Bello, Avenida República 275, Santiago, Chile. E-mail: sebastian.miranda@ unab.cl

balanced with the dispersion and ionic contributions as the stabilizing parts of the interaction,[45–47] acting as a driving force for orbital interactions among the metallic centers. From these studies, it is possible to demonstrate the importance of the dispersion term in the attractive interaction involved in the metal–metal equilibrium distance. Moreover, the same complexes show an electrostatic interaction *via* a dipole–dipole term that dominates at the equilibrium Au–Au distance, which is calculated from the summing of the induction and dispersion terms.[48,49] The experimental results in many studies can be explained using theoretical models described at the post-Hartree–Fock (MP2, SCS-MP2, CCSD(T)) and density functional theory (DFT) with dispersion levels.[10] In the case of bigger systems, the DFT method is normally preferred because of its better performance, although accuracy is sacrificed.[14]

We focused our attention on two types of gold complexes, where the formation of linear chains by gold(I) complexes are stabilized by unsupported Au(I)–Au(I) (d^{10}–d^{10}) ligand interactions and the absorption and luminescence processes take place at the gold centers. The first type corresponds to [AuCl(L)] models (L = CNR (R = –H, –CH$_3$, Cy)). Previous crystallographic studies on three isonitrile complexes [AuX(CNCy)] (CyNC = cyclohexyl isonitrile; X = Cl, Br, I),[50] have shown Au(I)–Au(I) distances from 338.9 pm to 371.8 pm, with absorption and luminescence bands at around 270 and 600 nm, respectively. All complexes showed a large Stokes shift (∼2.6 eV). This large Stokes shift is associated to the fact that the excited state adopts a distorted geometry with respect to the ground state. The experimental results indicate that the orange emission is due to a triplet excited state, typical of luminescent gold(I) compounds. There are no reported theoretical studies on these complexes.

The second type of system corresponds to [AuCl(CO)], for which photophysical studies have shown luminescent properties with emission at 663 nm from the solid,[51,52] and absorption at 250 nm. This complex also exhibits a red-orange luminescence with a large Stokes shift (∼2.1 eV), associated to aurophilic interactions between molecules in the excited state. In both compounds, self-association of two-coordinated gold(I) atoms that interact through an antiparallel geometry among the monomer units is observed. In the work of White-Morris *et al.*,[50] it was suggested that in the [AuX(CNCy)] (X = –Cl, –Br, –I) complex the interaction is not only limited to aurophilic bonding, since there is also a relevant intermolecular stabilizing contribution from an electrostatic interaction such as a dipolar interaction. It has been suggested that these structural properties have consequences in terms of the observed optical properties.

Herein, we focused on establishing a relationship between the aurophilic interactions and experimental geometries based on models of type [AuCl(L)]$_n$ (n = 2, 4) (L = CNR (R = –H, –CH$_3$, Cy); CO). Moreover, our second aim was to study the geometrical and optical properties at the post-Hartree–Fock (SCS-CC2) and DFT (PBE and B3LYP) levels on simplified models of the two types of complexes described above; namely [AuCl(CNR)] and [AuCl(CO)]. The light-absorption processes in

the complexes were studied using time-dependent density functional theory (TDDFT) calculations and by performing *ab initio* correlated calculations at the approximate scaled opposite-spin approximation second-order coupled cluster (SCS-CC2).

2. Theoretical models and calculations

2.1 Quantum chemical methods

We used the [AuCl(L)] models (L = CNR (R = –H, –CH$_3$, Cy); CO) (models **1** to **4** from Fig. 1) to model the aurophilic attractions of the [AuCl(L)]$_n$ (n = 2, 4) complexes shown in Fig. 2, defined as models **5** to **10**. The dimers and tetramers in Fig. 2 were built with an antiparallel orientation to simulate the experimental geometry.[50] The geometries were fully optimized at the scalar relativistic HF, MP2, SCS-MP2, CCSD(T), PBE (Perdew–Burke–Ernzerhof),[53] B3LYP,[54] PW91,[55] and M06L[56] levels in the gas phase for each fragment in the models. Grimme's dispersion correction was used to
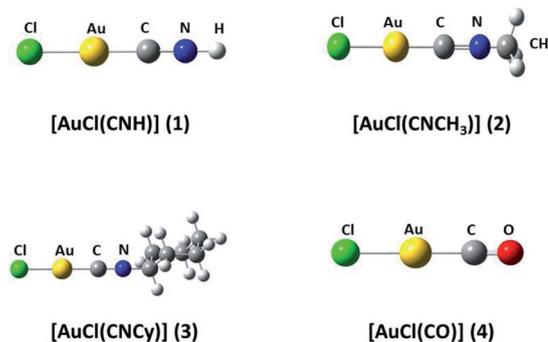

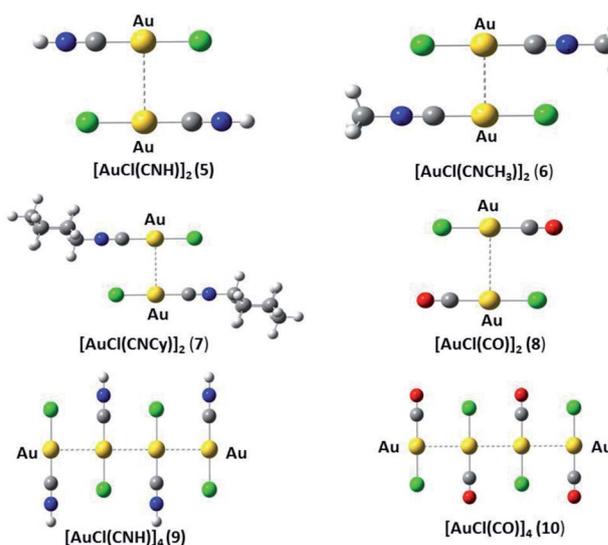**Fig. 1** Theoretical [AuCl(L)] models (L = CNR (R = –H, –CH$_3$, Cy); CO) **1–4**.

Fig. 2 Theoretical [AuCl(L)]$_n$ (n = 2, 4) models (**5–10**).

incorporate an accurate description of the weak forces when using the functionals, in what is nowadays known as the DFT-D3 level with the Becke–Johnson (BJ) damping function correction.[57,58] The interaction energy (ΔE_{int}) and geometric equilibrium distances (R_e) of the complexes were obtained using the counterpoise correction for the basis-set superposition error (BSSE),[59,60]

$$\Delta E = E_{AB}^{(AB)} - E_A^{(AB)} - E_B^{(AB)} \tag{1}$$

The calculations were carried out using the Turbomole 7.0,[61] and Gaussian 16 (ref. 62) program packages. We used the Turbomole program to obtain the optical properties, while the Gaussian program was used to obtain the equilibrium geometries and electronic properties. The 19 valence-electrons (VE) of the Au quasi-relativistic (QR) pseudo-potential (PP) of Andrae *et al.*[63] were employed. We used 2f and 3f2g-type polarization and diffuse functions for gold, respectively (α_f = 0.20, 1.19; α_f = 1.41, 0.40; 0.15, α_g = 1.20, 0.40). Also, the C, N, O, and Cl atoms were treated through PPs, using double-zeta basis sets with the addition of two d-type polarization functions.[64] A double-zeta basis set plus two p-type polarization functions were used for the H atoms.[65]

Single point calculations of the equilibrium geometries were used to study the excitation spectra by PBE and B3LYP. The excitation energy was obtained using the time-dependent perturbation theory approach (TD),[66] which is based on the random-phase approximation (RPA) method.[67] The TD calculations do not evaluate the spin–orbit splitting, and the values were averaged for the metallic atoms described by pseudopotentials. Moreover, excitation energies and oscillator strengths were calculated at the approximate second-order coupled cluster (CC2) level using the scaled opposite-spin approximation (SCS-CC2).[68,69] We used the equilibrium distance (R_e) estimated at the SCS-MP2 level to calculate the excitation spectrum at SCS-CC2. The SCS-MP2 methodology is an accurate and efficient tool for incorporating electronic correlation for the study of models at a low computational cost.[69] This method involves the Laplace transformation (LT) algorithm and the reduced-virtual-space (RVS) approximation. The RVS cut-off threshold was 60 eV.[70]

The optical properties are described from the theoretical calculations. The Stokes shifts described are the energy difference between the $S_0 \rightarrow S_1$ absorption and the $T_1 \rightarrow S_0$ emission ($S_0 \rightarrow S_1 \cdots T_1 \rightarrow S_0$).[70] Also, we used a second definition, which is the energy between the $S_0 \rightarrow T_1$ absorption and the $T_1 \rightarrow S_0$ emission ($S_0 \rightarrow T_1 \rightarrow S_0$).[71] This approach assumes that the spin-allowed transitions dominate the absorption spectra with weaker contributions from spin-forbidden transitions.

2.2 Theory of intermolecular forces

We can partition the interaction energy of eqn (2) as:

$$\Delta E = \Delta E(\text{SCF}) + \Delta E(\text{corr}) \tag{2}$$

where $\Delta E(\text{SCF})$ is the interaction energy evaluated from a self-consistent field (SCF) supermolecule calculation at the Hartree–Fock (HF) or DFT level. The second term, $\Delta E(\text{corr})$, is the electron correlation energy, which is a useful approximation to the dispersion energy at the MP2, SCS-MP2, CCSD(T) and DFT-D3 levels.[60] The total intermolecular potential V_{int} (ref. 72 and 73) can be partitioned into different contributions at long ranges [eqn (3)],[74] where the overlap between the molecular charge clouds is insignificant.

$$V_{int} = V_{short} + V_{elect} + V_{ind} + V_{disp} \tag{3}$$

where the four terms are the short-range (V_{short}), electrostatic (V_{elect}), induction (V_{ind}), and dispersion (V_{disp}) contributions. At short distances, repulsive effects arise due to the electron clouds of the species penetrating each other and leading to charge overlap. At long range, the electrostatic and induction terms are classical. Furthermore, the dispersion term also has long-range character. It is attractive, but requires a quantum mechanical interpretation.[74]

The Hartree–Fock or DFT term ($\Delta E(\text{HF})$) is associated with the sum of short-range (V_{short}), electrostatic (V_{elect}), and induction (V_{ind}) terms; while the $\Delta E(\text{corr})$ electron correlation term is associated with dispersion (V_{disp}).[74] Hence, we aimed to relate the intermolecular interaction at the equilibrium distance Au–Au with the properties of the isolated [AuCl(CNR)] and [AuCl(CO)] through the dipole moment (μ), polarizability (α), and first ionization potential (IP$_1$). The latter property was obtained from Koopmans' theorem.[75] The Au–Au interactions were studied using the specific configuration given for [AuCl(CNR)]$_2$ and [AuCl(CO)]$_2$ concerning their dipole moment, as shown in Fig. 2. All dimer models have a conformation with antiparallel orientation (180°).

We based this study on previously published work on [AuCl(L)]$_2$ dimers,[48] where the dipole–dipole, induction, and dispersion terms are relevant. For this particular case, the expressions for the intermolecular potential are outlined in the following equations.

$$V_{dipole-dipole} = -\left(\frac{\mu^2}{R^3}\right) \tag{4}$$

$$V_{induction} = \frac{1}{2}\left(\frac{\alpha\mu^2}{R^6} + \frac{2}{3}\frac{(\alpha_\parallel - \alpha_\perp)}{R^6}\right) \tag{5}$$

$$V_{dispersion} = -\frac{3}{4}\frac{IP_1}{R^6}\left(\alpha^2 - \frac{1}{3}\alpha(\alpha_\parallel - \alpha_\perp)\right) \tag{6}$$

3. Results and discussion

3.1 Aurophilic attractions and intermolecular forces

The [AuCl(L)]$_2$ dimer systems (L = CNR (R = –H, –CH$_3$, Cy) and CO (models **5–8**) were used for modeling the aurophilic attractions. To compare and systemize the analysis of the aurophilic intermolecular interactions, we have included the results in Tables 1 and 2, where we summarize the interaction

Table 1 Optimized Au–Au distance, R_e, for models **1** and **2** at the different levels. Equilibrium distance R_e in pm; interaction energy $V(R_e)$ in kJ mol^{-1}

Monomer	Method	Au (basis)	R_e	$V(R_e)$
[AuCl(CNH)]$_2$ (**5**)	HF	2f	402.8	−23.8
	MP2	2f	352.2	−42.3
	SCS-MP2	2f	362.7	−34.9
	CCSD(T)	2f	360.9	−34.8
	HF	3f2g	405.7	−23.9
	MP2	3f2g	346.7	−44.6
	SCS-MP2	3f2g	356.6	−37.2
	CCSD(T)	3f2g	360.7	−35.6
	PW91	3f2g	369.3	−23.3
	M06L	3f2g	352.3	−33.0
	PBE-D3	3f2g	352.6	−38.1
	B3LYP-D3	3f2g	350.8	−46.0
	PBE[a]	3f2g	352.6	−23.3
	B3LYP[a]	3f2g	350.8	−17.7
[AuCl(CNCH$_3$)]$_2$ (**6**)	HF	2f	391.9	−28.6
	MP2	2f	352.5	−47.3
	SCS-MP2	2f	358.8	−40.3
	CCSD(T)	2f	363.7	−40.6
	HF	3f2g	393.2	−28.0
	MP2	3f2g	346.0	−50.4
	SCS-MP2	3f2g	354.4	−42.5
	CCSD(T)	3f2g	359.8	−42.5
	PW91	3f2g	365.3	−28.8
	M06L	3f2g	347.9	−41.0
	PBE-D3	3f2g	347.8	−46.8
	B3LYP-D3	3f2g	346.9	−54.2
	PBE[a]	3f2g	347.8	−29.3
	B3LYP[a]	3f2g	346.9	−30.9

[a] Single point at R_e in D3.

Table 2 Optimized Au–Au distance, R_e, for models **3** and **4** at the different levels. Equilibrium distance R_e in pm; interaction energy $V(R_e)$ in kJ mol^{-1}

Monomer	Method	Au (basis)	R_e	$V(R_e)$
[AuCl(CNCy)]$_2$ (**7**)	HF	2f	401.1	−27.1
	MP2	2f	349.8	−46.4
	SCS-MP2	2f	358.8	−40.3
	CCSD(T)	2f	360.5	−39.1
	HF	3f2g	399.4	−26.2
	MP2	3f2g	344.6	−49.7
	SCS-MP2	3f2g	354.4	−42.5
	PW91	3f2g	368.3	−26.5
	M06L	3f2g	349.5	−38.4
	PBE-D3	3f2g	347.3	−45.6
	B3LYP-D3	3f2g	345.8	−54.2
	PBE[b]	3f2g	347.3	−26.9
	B3LYP[b]	3f2g	345.8	−19.8
[AuCl(CO)]$_2$ (**8**)	HF	2f	393.1	−12.6
	MP2	2f	352.3	−30.9
	SCS-MP2	2f	362.8	−25.5
	CCSD(T)	2f	363.6	−25.3
	HF	3f2g	394.7	−11.8
	MP2	3f2g	344.2	−33.8
	SCS-MP2	3f2g	356.9	−28.0
	CCSD(T)	3f2g	356.4	−26.9
	PW91	3f2g	361.7	−15.5
	M06L	3f2g	343.9	−24.4
	PBE-D3	3f2g	347.1	−29.2
	B3LYP-D3	3f2g	345.9	−35.8
	PBE[b]	3f2g	347.1	−14.9
	B3LYP[b]	3f2g	345.9	−8.4
[AuCl(CNCy)][a]	Exp.[50]		339	
			359	
[AuCl(CO)]	Exp.[52]		338	

[a] Cy is cyclohexyl. [b] Single point at R_e in D3.

energies and Au–Au distances. In this context, the results reported in this study using the MP2, SCS-MP2 and CCSD(T) methods are at the same level as reported in the literature for both the interaction energy and the geometry.[50,52] We can verify that using the Hartree–Fock (HF) method, there is a long-distance Au–Au attraction (approximately 400 pm) with a stabilizing interaction energy in all dimers. This result is not surprising since the antiparallel orientation of the dimers favours such attraction *via* the interaction of the dipole moments, which has already been reported for a classical [(ClAuPH$_3$)$_2$] system, where the dipole term dominates.[48] We can also appreciate that when going from a 2f to a 3f2g basis for gold, the Au–Au interaction energy increases, and the Au–Au distance slightly decreases as a consequence. As is known,[13,14] the MP2 method tends to overestimate the interaction energy and to shorten the Au–Au distance. The CCSD(T) method provides a better description, with a lower interaction energy and a longer Au–Au distance than obtained at the MP2 level. This trend can be observed in all complexes from their interaction energies and geometric parameters. The novelty in these results comes from the values obtained with the SCS-MP2 method, which generates similar accuracy to CCSD(T) but at a lower computational expense.

For the DFT calculations, we used the larger 3f2g basis set. It has been shown that there are no significant differences

between these methodologies. For the PBE and B3LYP functionals, only after the dispersion corrections (D3) were included were the interaction energy and Au–Au distances comparable to those obtained at the MP2 level. At the same time, the PW91 and M06L functionals showed different behaviour, as shown in Table 1. When we used PW91, it provided a poor description of the interaction energy and Au–Au distance. Meanwhile, results obtained using the M06L functional are similar to those obtained at the SCS-MP2 and CCSD(T) levels.

Using the results in Tables 1 and 2, we applied the theory of intermolecular forces to obtain an estimate of the aurophilic attractions and the electrostatic (dipole–dipole and inductive) term. At the equilibrium distance in each dimer, the aurophilic attraction is obtained by subtracting the $V(R_e)$ from the Hartree–Fock (HF) calculation at the MP2, SCS-MP2, and CCSD(T) levels of theory. The amount that remains from the subtraction is associated with the dipole–dipole and inductive terms. Meanwhile, at the PBE and B3LYP levels, this contribution comes directly from the D3 term, and the results are listed in Table 3. The [AuCl(CNR)]$_2$ dimers showed that the aurophilic interaction coming from the dipole–dipole and the inductive terms are important. At the MP2 level, the aurophilic attraction is

Table 3 Decomposition interaction energy $V(R_e)$ in the equilibrium distance (R_e) by aurophilic (dispersion) and electrostatic (dipole–dipole and inductive) terms. The energies are in kJ mol^{-1} and distances in pm

Monomer	Method	Au (basis)	R_e	Aurophilic	ΔE_{elect}
[AuCl(CNH)]$_2$ (**5**)	MP2	2f	352.2	−24.9	−17.4
	SCS-MP2	2f	362.7	−14.3	−20.6
	CCSD(T)	2f	360.9	−13.7	−21.2
	MP2	3f2g	346.7	−31.6	−13.0
	SCS-MP2	3f2g	356.6	−17.2	−18.4
	CCSD(T)	3f2g	360.7	−20.2	−17.1
	PBE-D3	3f2g	352.6	−14.8	−23.3
	B3LYP-D3	3f2g	350.8	−28.3	−17.7
[AuCl(CNCH$_3$)]$_2$ (**6**)	MP2	2f	352.5	−25.4	−21.9
	SCS-MP2	2f	358.8	−15.1	−25.5
	CCSD(T)	2f	363.7	−16.1	−24.1
	MP2	3f2g	346.0	−32.3	−18.0
	SCS-MP2	3f2g	354.4	−20.8	−21.3
	CCSD(T)	3f2g	359.8	−18.9	−23.6
	PBE-D3	3f2g	347.8	−17.6	−29.3
	B3LYP-D3	3f2g	346.9	−23.3	−30.9
[AuCl(CNCy)]$_2$ (**7**)	MP2	2f	349.8	−28.8	−17.6
	SCS-MP2	2f	358.8	−20.3	−19.9
	CCSD(T)	2f	360.5	−17.3	−21.8
	MP2	3f2g	344.6	−35.4	−14.3
	SCS-MP2	3f2g	354.4	−26.3	−16.3
	PBE-D3	3f2g	347.3	−18.7	−26.4
	B3LYP-D3	3f2g	345.8	−34.4	−19.8
[AuCl(CO)]$_2$ (**8**)	MP2	2f	352.3	−23.9	−7.0
	SCS-MP2	2f	362.8	−15.7	−9.8
	CCSD(T)	2f	363.6	−15.3	−9.9
	MP2	3f2g	344.2	−31.1	−2.7
	SCS-MP2	3f2g	356.9	−20.7	−7.3
	CCSD(T)	3f2g	356.4	−19.7	−7.2
	PBE-D3	3f2g	347.1	−14.2	−14.9
	B3LYP-D3	3f2g	345.9	−27.4	−8.4

Table 5 Finite field calculations of the electric properties of [AuClX] (X = −CNH, −CNCH$_3$, −CNCy, CO) monomers at the MP2 level. All values are in au

Properties	[AuCl(CNH)]	[AuCl(CNCH$_3$)]	[AuCl(CNCy)]	[AuCl(CO)]
μ	3.4907	4.0816	4.4677	1.6652
α	62.279	76.7312	129.8382	57.0902
$\alpha_\perp$	42.5394	52.3356	95.3189	39.9445
$\alpha_\parallel$	101.7605	125.5225	193.3875	91.3818
IP1	0.3862	0.3776	0.3744	0.4125

each dimer, with the results summarized in Table 4. This was complemented by the determination of the electronic properties of each monomer, as listed in Table 5. For the [AuCl(CNR)]$_2$ complex, the most important term is the dipole–dipole interaction (49% to 73%). However, for [AuCl(CNCy)]$_2$ the dispersion term is relevant due to a high polarizability (α) (35%). This complex has been experimentally synthesized,[50] from which it was observed that the geometry of the complex shows an antiparallel disposition of the monomers [AuCl(CNCy)]. This suggests that the dipolar term would be relevant in the orientation of the complex. However, the [AuCl(CO)]$_2$ dimer shows that the dipole–dipole (50%) and dispersion (43%) terms are of similar magnitude because the polarization of the monomer is low. Hence, both terms are equivalent in magnitude. The [AuCl(CNR)]$_2$ dimers show a high polarization reflected in a more relevant dispersion term.

3.2 Optical properties: absorption spectra

UV-Vis spectra have been calculated at the SCS-CC2 level. Also, the excitation energies of the models were calculated at the TDDFT level using the PBE-D3 and B3LYP-D3 functionals with the purpose of comparing their performance with respect to the SCS-CC2 results. We calculated the allowed spin-singlet transition for these systems based on the ground-state structures of the [AuCl(L)]$_n$ ($n = 1, 2, 4$) models, with the objective being to evaluate the electronic structure of the excited state *via* direct electronic excitations. The allowed transitions are listed in Table 6 for [AuCl(CNR)]$_n$ in models **1**, **5–7**, and **9**, and Table 7 shows the excitation energies of [AuCl(CO)]$_n$ in models **4**, **8**, and **10**.

We considered only the strong transitions obtained at the SCS-CC2 level in the discussion of the properties of the excited states since they are in good agreement with the experimental data, and the states are easily identified by comparing the excitation energies with the ones calculated at the other levels of theory. We will discuss the properties of the models **1**, **5–7**, and **9** and [AuCl(CO)]$_n$ models **4**, **8**, and **10**. The simulated spectra of all of the models are shown in Fig. 3–5. The most important molecular orbitals for describing the electronic transitions are shown in Fig. 6–9.

[AuCl(CNR)]$_n$ ($n = 1, 2, 4$; R = −H, −CH$_3$, −Cy). The gold complex shows an experimental spectrum with a characteristic band at 280 nm in the solid state. When we increase the size of the models from one to four units, regardless of the method

overestimated, while at the SCS-MP2 and CCSD(T) it decreases. The same behaviour was observed for the DFT methods. Among the systems here studied, the [AuCl(CO)]$_2$ dimer (**8**) is a special case. The results show that the aurophilic interaction is the most important term, although the electrostatic term is not negligible.

To gain insight on the origin of the intermolecular forces present in the systems under study, we calculated the contributions to the interaction energy represented by eqn (4)–(6) to estimate the dipole–dipole, inductive, and dispersion terms. The contributions of these three forces at the Au–Au equilibrium distance were estimated at the MP2 level for

Table 4 Application of the intermolecular forces in the [AuClX] (X = −CNH, −CNCH$_3$, −CNCy, CO) dimers using the equilibrium distance (R_e) and electronic properties from table at the MP2 level. All values are in kJ mol^{-1}

Properties	$V_{dipole-dipole}$	V_{ind}	V_{disp}
[AuCl(CNH)]$_2$	−108.4 (73%)	−18.7 (13%)	−21.3 (14%)
[AuCl(CNCH$_3$)]$_2$	−147.8 (69%)	−31.4 (15%)	−34.1 (16%)
[AuCl(CNCy)]$_2$	−181.2 (49%)	−61.2 (15%)	−129.0 (35%)
[AuCl(CO)]$_2$	−24.6 (50%)	−3.8 (8%)	−21.2 (43%)

Paper

Table 6   The strongest singlet excitation energies calculated for models 1–4 compared to experimental data.[40] The excitation energies and oscillator strengths calculated at the TDDFT and CC2 levels. Molecular orbital contributions and the character of the transitions are also given

System	Method	λ_{calc}/nm	f^a	Contribution^b	Transition type
[AuCl(CNH)] (1)	SCS-CC2	199	0.4973	18a → 20a (35)	LLCT($p_z \to \pi^*$)
				17a → 21a (35)	LLCT($p_z \to \pi^*$)
	PBE	265	0.2550	18a → 20a (45)	LLCT($p_z \to \pi^*$)
				17a → 19a (45)	LLCT($p_z \to \pi^*$)
	B3LYP	222	0.223	17a → 20a (44)	LLCT($p_z \to \pi^*$)
				18a → 19a (44)	LLCT($p_z \to \pi^*$)
[AuCl(CNH)]$_2$ (5)	SCS-CC2	238	0.4243	36a → 40a (61)	MLMLCT($d^*_{xz} + p_z$)→($sp_z + p_z$)
				36a → 38a (21)	MLMLCT($d^*_{xz} + p_z$)→(sp_z)
	PBE	238	0.2551	36a → 40a (44)	MLMLCT($d^*_{xz} + p_z$)→($sp_z + p_z$)
				36a → 38a (21)	MLMLCT($d^*_{xz} + p_z$)→(sp_z)
	B3LYP	257	0.1296	36a → 37a (85)	MLMLCT($d^*_{xz} + p_z$)→($sp_z + p_z$)
		241	0.1341	35a → 37a (57)	MLMLCT($d^*_{xz} + p_z$)→(sp_z)
[AuCl(CNH)]$_4$ (9)	SCS-CC2	263	1.3934	72a → 78a (71)	MLMLCT($d^*_{xz} + p_z$)→($sp_z + p_z$)
				72a → 74a (21)	MLMLCT($d^*_{xz} + p_z$)→(sp_z)
	PBE	321	0.4311	72a → 73a (96)	MLMLCT($d^*_{xz} + p_z$)→($sp_z + p_z$)
	B3LYP	270	0.7256	72a → 73a (95)	MLMLCT($d^*_{xz} + p_z$)→($sp_z + p_z$)
[AuCl(CNCH$_3$)]$_2$ (6)	SCS-CC2	217	0.3767	42a → 46a (53)	MLMLCT($d^*_{z^2} + p_z$)→($sp_z + p_z$)
				42a → 44a (20)	MLMLCT($d^*_{xz} + p_z$)→(sp_z)
	PBE	228	0.382	40a → 46a (34)	MLMLCT($d^*_{z^2} + p_z$)→($sp_z + p_z$)
				39a → 45a (20)	MLMLCT($d^*_{xz} + p_z$)→(sp_z)
	B3LYP	242	0.1563	42a → 43a (84)	MLMLCT($d^*_{xz} + p_z$)→(sp_z)
[AuCl(CNCy)]$_2$ (7)	SCS-CC2	238	0.3559	70a → 74a (53)	MLMLCT($d^*_{z^2} + p_z$)→($sp_z + p_z$)
				70a → 73a (14)	MLMLCT($d^*_{xz} + p_z$)→(sp_z)
	PBE	234	0.5375	69a → 74a (34)	MLMLCT($d^*_{z^2} + p_z$)→($sp_z + p_z$)
				67a → 73a (25)	MLMLCT($d^*_{xz} + p_z$)→(sp_z)
	B3LYP	245	0.1590	67a → 71a (92)	MLMLCT($d^*_{z^2} + p_z$)→($sp_z + p_z$)
		234	0.1094	66a → 71a (57)	MLMLCT($d^*_{xz} + p_z$)→(sp_z)
[AuCl(CNCy)]$_2$	Solid[50]	280			

^{a} Oscillator strength. ^{b} Values are |coeff.|$^2 \times$ 100.

used, we observe a blue-shift in the theoretical absorption bands with respect to the experimental spectrum for the [AuCl(CNH)]$_n$ (1, 2, 4) models. The details on the electronic transitions and their respective orbital contributions are listed in Table 6. The calculated spectra show a principal transition of the changes depending on the size of the model. The [AuCl(CNH)]$_n$ (n = 2, 4) models 5 and 9 are approach the experimental value. However, as the experimental complexes form oligomeric structures, the limited number of subunits from our models allowed us to obtain agreement at the semiquantitative level, also explaining the shift between the theoretical and experimental bands. Models 5 and 9 have one principal transition at 238 and 263 nm, respectively; which can be essentially attributed to a metal–metal charge transfer (MMCT), and are mainly centred among the gold atoms from antibonding to bonding orbitals. The active molecular orbitals in the electronic transition are shown in Fig. 6. Regarding model 1, transitions are generated between gold and ligands, as it is only a basic unit, and produce a short wavelength band.

When we studied the [AuCl(CNR)]$_2$ (R = –CH$_3$, –Cy) system represented by models 6 and 7, with model 7 being a representation of the experimental complex; we can observe that at the SCS-CC2 level the main band is a consequence of the transitions at 217 and 238 nm for models 6 and 7, respectively. Both bands correspond to those observed in models 5 and 9, which can be attributed to MMCT, as depicted in Fig. 7. The most essential contribution corresponds to orbitals centred on gold atoms with strong bonding character among these atoms.

[AuCl(CO)]$_n$ (n = 1, 2, 4). The theoretical transitions of the systems (models 4, 8, and 10) and experimental spectroscopic absorption data are summarized in Table 7. The experimental spectra in the solvent phase (acetonitrile) show intense absorption bands at 208 and 220 nm,[41] with one shoulder at 250 nm. From Table 7, model 4 can be seen to properly describe the experimental spectrum at the SCS-CC2 level for two transitions: 204 and 220 nm. Meanwhile, the DFT results show poor prediction of the experimental data. The spectra calculated at the SCS-CC2 level show theoretical transitions in Fig. 5. The transitions are generated between gold and the ligands (see Fig. 8).

Using the larger models 8 and 10, it is possible to appreciate the increase in the transition band (Fig. 5). The principal transitions can be assigned to 36a → 38a (240 nm) and 72a → 74a (263 nm) for models 8 and 10, respectively. These bands

Table 7 The strongest singlet excitation energies calculated for models 1–4 compared to experimental data.[40] The excitation energies and oscillator strengths calculated at the TDDFT and CC2 levels. Molecular orbital contributions and the character of the transitions are also given

System	Method	λ_{calc}/nm	f^a	Contribution^b	Transition type
[AuCl(CO)] (4)	SCS-CC2	220	0.0652	16a → 19a (67)	MLMLCT($d^*_{z^2} + p_x$) → (π^*)
		213	0.0641	16a → 20a (69)	MLMLCT($d^*_{z^2} + p_x$) → (π^*)
		204	0.5017	17a → 20a (41)	MLMLCT($d^*_{xz} + p_z$) → (π^*)
				18a → 19a (40)	MLMLCT($d^*_{yz} + p_y$) → (π^*)
	PBE	260	0.2231	17a → 19a (46)	MLMLCT($d^*_{xz} + p_y$) → (π^*)
				17a → 20a (46)	MLMLCT($d^*_{xz} + p_z$) → (π^*)
		233	0.2462	17a → 19a (48)	MLMLCT($d^*_{xz} + p_y$) → (π^*)
				18a → 20a (48)	MLMLCT($d^*_{yz} + p_y$) → (π^*)
	B3LYP	232	0.2462	17a → 19a (48)	MLMLCT($d^*_{xz} + p_y$) → (π^*)
				18a → 20a (48)	MLMLCT($d^*_{yz} + p_y$) → (π^*)
		189	0.0342	17a → 21a (45)	MLMLCT($d^*_{xz} + p_y$) → (π^*)
				18a → 21a (45)	MLMLCT($d^*_{yz} + p_y$) → (π^*)
[AuCl(CO)]$_2$ (8)	SCS-CC2	240	0.3982	36a → 38a (65)	MLMLCT($d^*_{xz} + p_z$) → ($sp_z + p_z$)
		201	0.3739	33a → 38a (35)	MLMLCT($d^*_{xz} + p_z$) → ($sp_z + p_z$)
				35a → 37a (28)	MLMLCT($d^*_{xy} + p_x$) → ($sp_x + p_x$)
	PBE	273	0.1167	32a → 37a (90)	MLMLCT($d^*_{xy} + p_x$) → ($sp_x + p_x$)
		251	0.3310	33a → 40a (33)	MLMLCT($d^*_{xz} + p_z$) → (p_z)
				34a → 39a (21)	MLMLCT($d^*_{xy} + p_x$) → (p_x)
	B3LYP	245	0.1279	32a → 37a (42)	MLMLCT($d^*_{xy} + p_x$) → ($sp_x + p_x$)
				34a → 39a (31)	MLMLCT($d^*_{xy} + p_x$) → (p_x)
		220	0.3318	33a → 40a (50)	MLMLCT($d^*_{xz} + p_z$) → (p_z)
				34a → 39a (22)	MLMLCT($d^*_{xy} + p_x$) → (p_x)
[AuCl(CO)]$_4$ (10)	SCS-CC2	263	1.2921	72a → 74a (77)	MLMLCT($d^*_{xz} + p_z$) → ($sp_z + p_z$)
	PBE	356	0.4395	72a → 73a (95)	MLMLCT($d^*_{xz} + p_z$) → ($sp_z + p_z$)
	B3LYP	298	0.7252	72a → 73a (96)	MLMLCT($d^*_{xz} + p_z$) → ($sp_z + p_z$)
[AuCl(CO)]	CH$_3$CN solvent[51]	208; 220; 250			

^{a} Oscillator strength. ^{b} Values are $|coeff.|^2 \times 100$.

correspond to MMCT (see Fig. 9), very similar to those obtained for the [AuCl(CNR)]$_2$ (R = –CH$_3$, –Cy) systems represented by models 6 and 7 and described in the previous section.

3.3 Absorption and emission energies

The obtained absorption and emission energies, wavelengths and the corresponding Stokes shifts for the monomers and dimers are listed in Table 8. For the monomers of the [AuCl(CNH)] (1) and [AuCl(CO)] (4) models, the calculations show some differences between the absorption energies depending on the method used. The $S_0 \rightarrow S_1$ absorption energies calculated at the SCS-CC2 are ~0.5–1.2 eV higher than those obtained at the B3LYP and PBE levels. However, the $T_1 \rightarrow S_0$ emission energies are very close among the three methods. The calculations yielded a large Stokes shift in both methods used here of 3.4–4.9 eV, without significant changes.

We carried out similar analysis for the dimers of [AuCl(CNH)]$_2$ (5) and [AuCl(CO)]$_2$ (8). The absorption energies of the dimers are red-shifted ~0.30–1.2 eV compared to the $S_0 \rightarrow S_1$ for the corresponding monomers. The emission energies for [AuCl(CNH)]$_2$ are ~0.14–1.4 eV higher for the

monomer, while PBE remains almost constant and very close to the experimental luminescence spectra. Also, the emission energies for [AuCl(CO)]$_2$ are ~0.5–1.5 eV higher for the monomer.

The calculations show that the emission wavelength for the dimers is expected to be in the range of 400–650 nm, which agrees reasonably well with the experimental data for the solid-state material of both complexes.[50] For the [AuCl(NCCy)] complex in solid state, the absorption and emission luminescence bands are around 270 and 600 nm, with a large Stokes shift (~2.6 eV).[50] The theoretical result at the PBE level is in agreement with the calculated absorption and spin-forbidden emission at 277 and 662 nm, respectively. Also, the Stokes shift $S_0 \rightarrow T_1 \rightarrow S_0$ is 2.54 eV. However, the [AuCl(CO)] solid showed absorption and emission bands at 250 and 663 nm, respectively, with a large Stokes shift of ~2.1 eV. The B3LYP and PBE results are in good agreement with the experimental data in the ranges of 257 and 313 nm for the absorption; and within 532 and 604 nm for emission. The Stokes shifts are in the range of 2.1–2.5 eV. Also, the comparison of the absorption and emission energies calculated at the DFT and the CC2 levels showed that the former
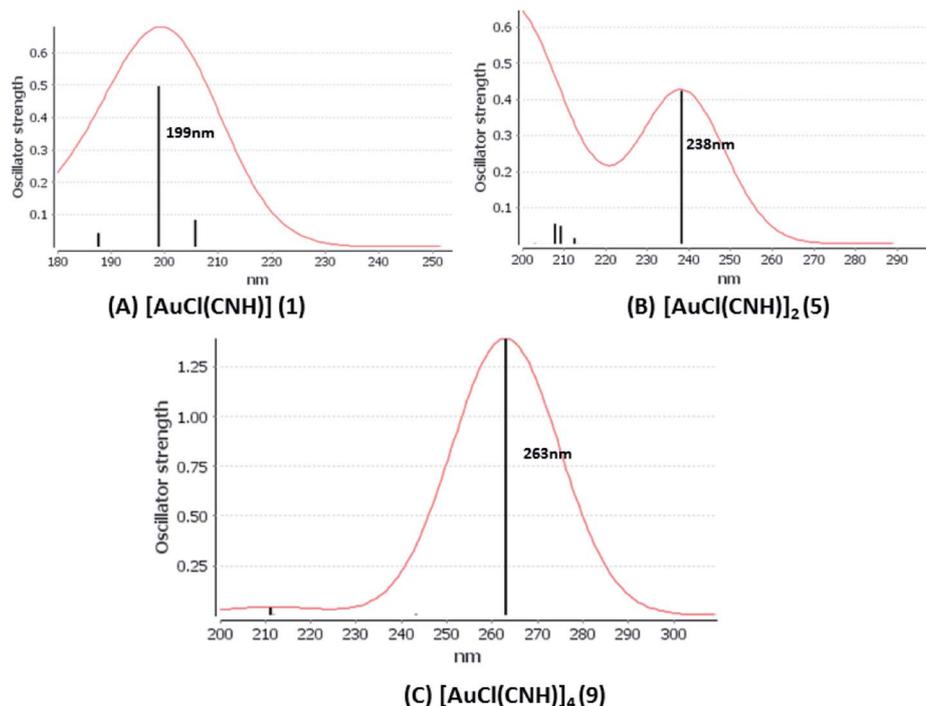
(A) [AuCl(CNH)] (1)

(B) [AuCl(CNH)]₂ (5)

(C) [AuCl(CNH)]₄ (9)

Fig. 3 Electronic spectra at the SCS-CC2 level calculated for $[AuCl(CNH)]_n$ ($n = 1, 2, 4$) models (**1**, **5**, and **9**).

(A) [AuCl(CNCH₃)]₂ (6)

(B) [AuCl(CNCy)]₂ (7)
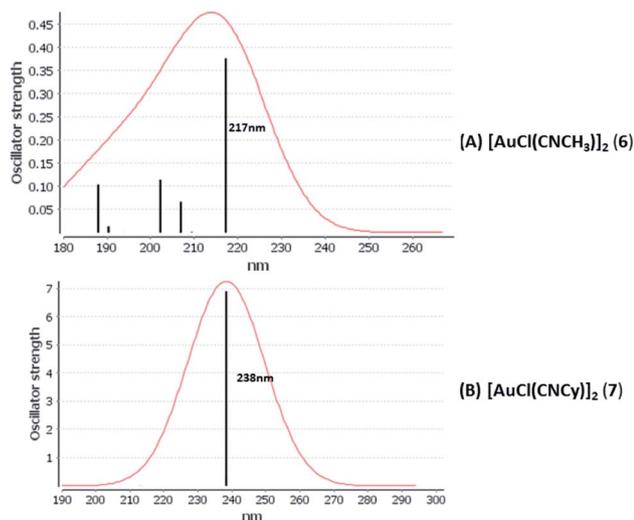
Fig. 4 Electronic spectra at the SCS-CC2 level calculated for $[AuCl(CNR)]_2$ (R = –CH₃, –Cy) models (**6** and **7**).

underestimates the excitation energies with respect to CC2, although all the results show a similar trend.

From an experimental point of view, the large Stokes shifts can be attributed to the existence of exciplex formation with a shortening of the Au–Au distance in the excited state. Table 9 summarizes the Au–Au distance for the ground state and excited states (S_1 and T_1). We optimized the geometry for both excited states. In all methods used, we can see that for the $[AuCl(CNH)]_2$ (**5**) and $[AuCl(CO)]_2$ (**8**) dimer models, there is

a strong shortening of the Au–Au distance. It was already possible to visualize this situation, when in the previous section it was shown that the main transition in the absorption spectra corresponded to a molecular orbital with strong bonding character among the gold atoms. This theoretical result confirms the predictions made by the Balch group in their experimental work on [AuX(CNCy)] complexes in the solid state.[50]

3.4 Aurophilic effect and optical properties

The aurophilic interactions are considered in most complexes to be mainly responsible for the electronic spectroscopic features, which have been proven to be highly dependent on the Au–Au distance.[48] The complexes herein studied show two important attractive forces dominating the Au–Au attraction: dipole–dipole and dispersion. In this context, the dipole–dipole interaction is responsible for the formation of an antiparallel configuration between the monomeric units, and thus, for their final geometry. According to our results, this type of configuration determines the optical properties of the systems because it allows a shortening of the Au–Au distances. It has been shown to be an essential structural feature that defines the absorption and emission bands behavior of the complexes. The $[AuCl(CNR)]_2$ (R = –H, –CH₃, –Cy) and $[AuCl(CO)]_2$ complexes show that the principal band is MMCT centered on the gold atoms for the absorption process. However, the emission energy shows a large Stokes shift that can be attributed to the existence of exciplex formation with shortening of the Au–Au distance in the excited state.
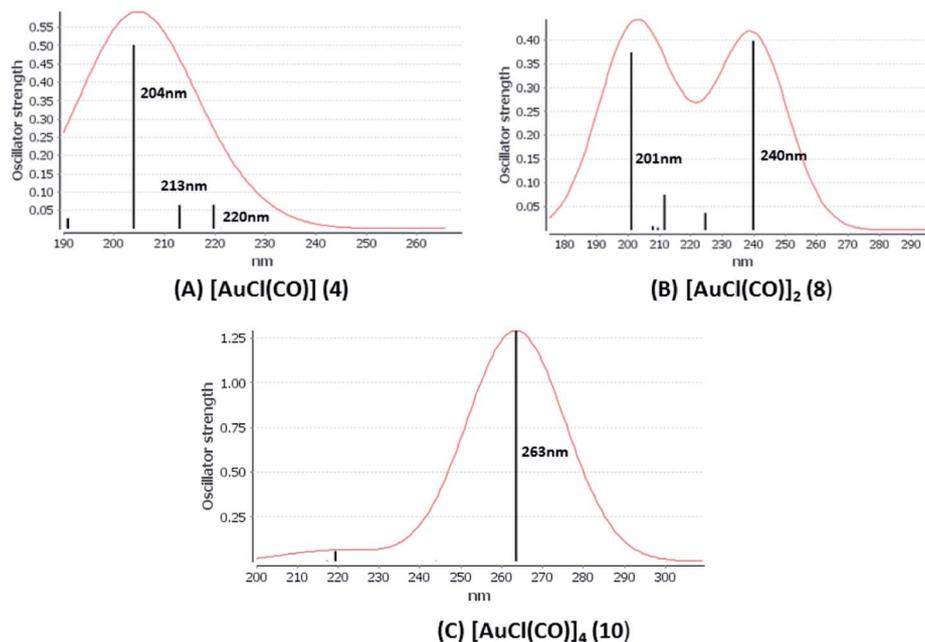
Fig. 5 Electronic spectra at the SCS-CC2 level calculated for [AuCl(CO)]$_n$ ($n = 1, 2, 4$) models (**4**, **8**, and **10**).
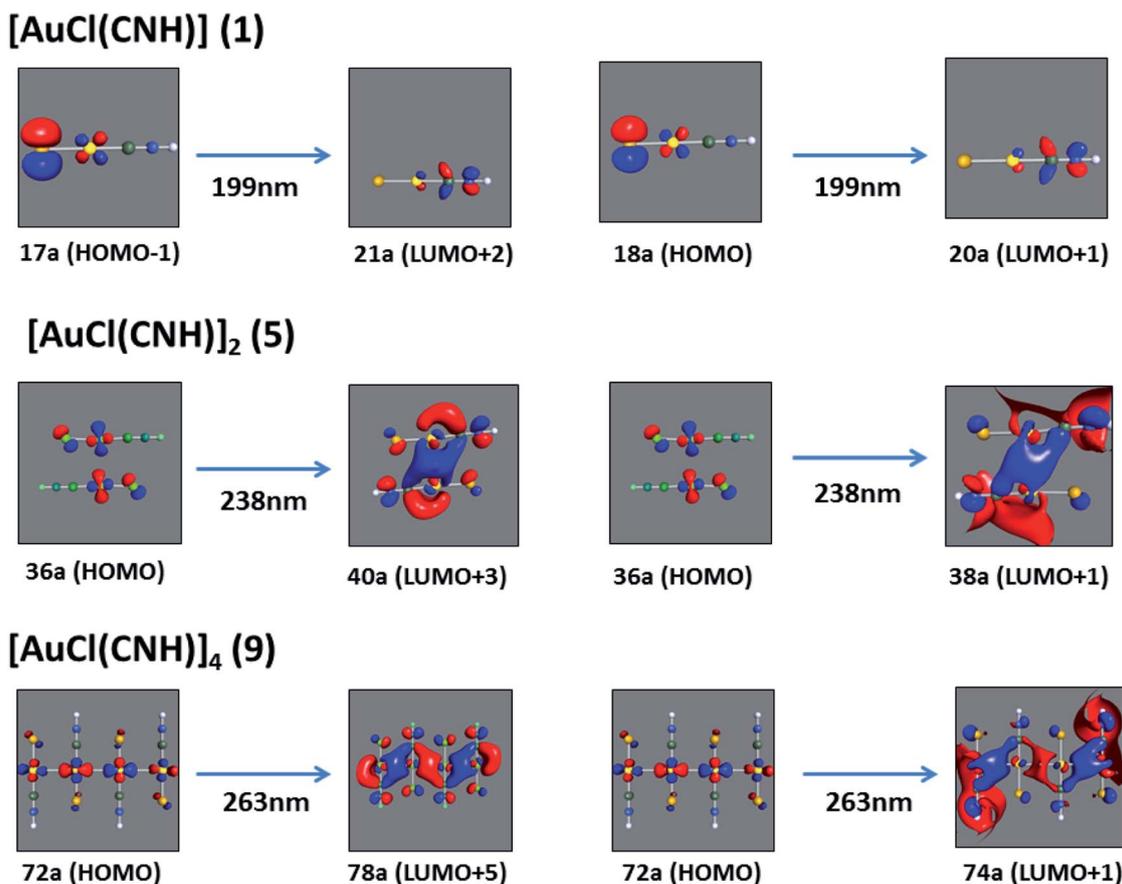

Fig. 6 Most important active molecular orbitals in the electronic transitions of the [AuCl(CNH)]$_n$ ($n = 1, 2, 4$) models (**1**, **5**, and **9**) at the SCS-CC2 level.

[AuCl(CNCH₃)]₂ (6)

42a (HOMO) → 217nm → 46a (LUMO+3)

[AuCl(CNCy)]₂ (7)

70a (HOMO) → 238nm → 74a (LUMO+3)

Fig. 7 Most important active molecular orbitals in the electronic transitions of the [AuCl(CNR)]₂ (R = −CH₃, −Cy) models (**6** and **7**) at the SCS-CC2 level.

In summary, taking into account the previous sections, although the aurophilic interaction is not relevant in the estimation of the direct electronic properties, it is mainly the equilibrium distances in the ground and first electronic state that define the optical properties of the complexes studied.

4.   Conclusion

The main results presented in this study point toward the relationship among the intermolecular interaction energy, the gold–gold distance in dimers of various [AuCl(L)] systems, and their optical properties. The dominant terms are related to the properties of the monomers, and the antiparallel orientations of dimers show that the dipole–dipole and dispersion terms are relevant. For the models studied, the aurophilic attraction is composed of both terms. The dipole–dipole term fixes the antiparallel geometries in the dimers, which explains the experimental results and determines the optical properties in the complexes. Excitation energies of monomers, dimers, and tetramers calculated at the SCS-CC2 level agree well with the experimental excitation spectra. The SCS correction in the MP2 energy allowed a high efficiency method to be used at a low cost. It was shown that intermetallic interactions are mainly responsible for the MMCT in dimers and tetramers. Moreover, the calculated absorption and emission energies reproduce experimental behaviour with large Stokes shifts in the dimers at the SCS-CC2 and DFT levels. Finally, all models show strong

[AuCl(CO)] (4)

16a (HOMO-2) → 220nm → 19a (LUMO)

16a (HOMO-2) → 213nm → 20a (LUMO+1)

17a (HOMO-1) → 204nm → 20a (LUMO+1)   17a (HOMO-1) → 204nm → 20a (LUMO+1)

Fig. 8 Most important active molecular orbitals in the electronic transitions of the [AuCl(CO)] model (**4**) at the SCS-CC2 level.

Fig. 9 Most important active molecular orbitals in the electronic transitions of the $[AuCl(CO)]_n$ ($n = 2, 4$) models (**8** and **10**) at the SCS-CC2 level.
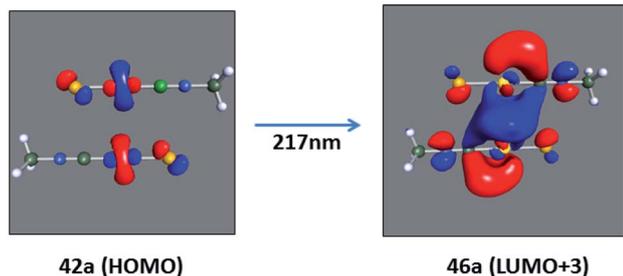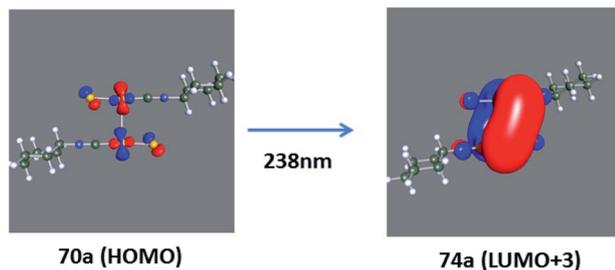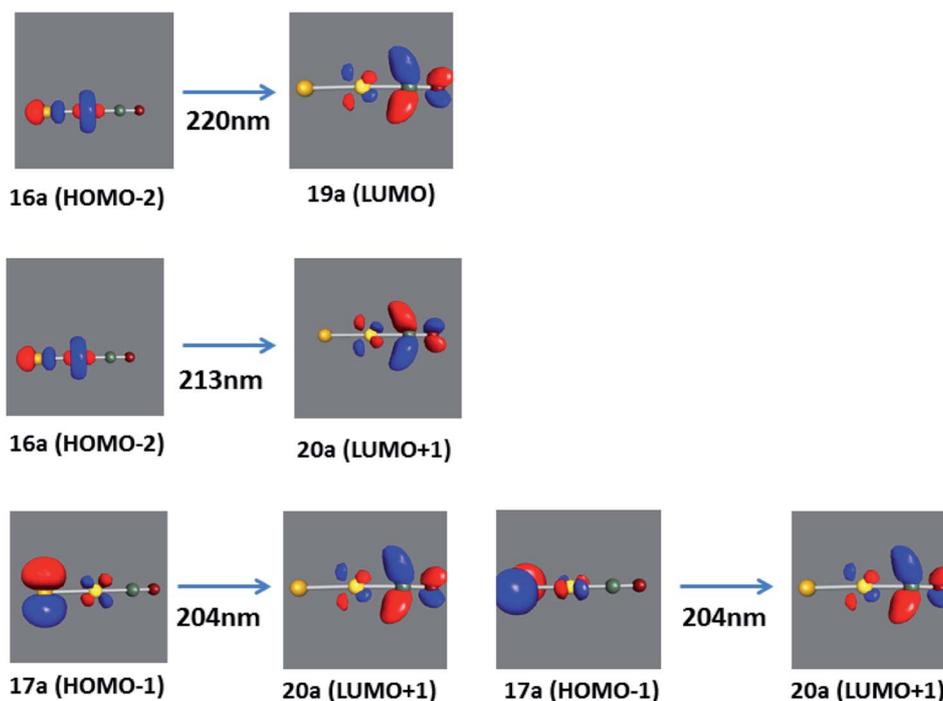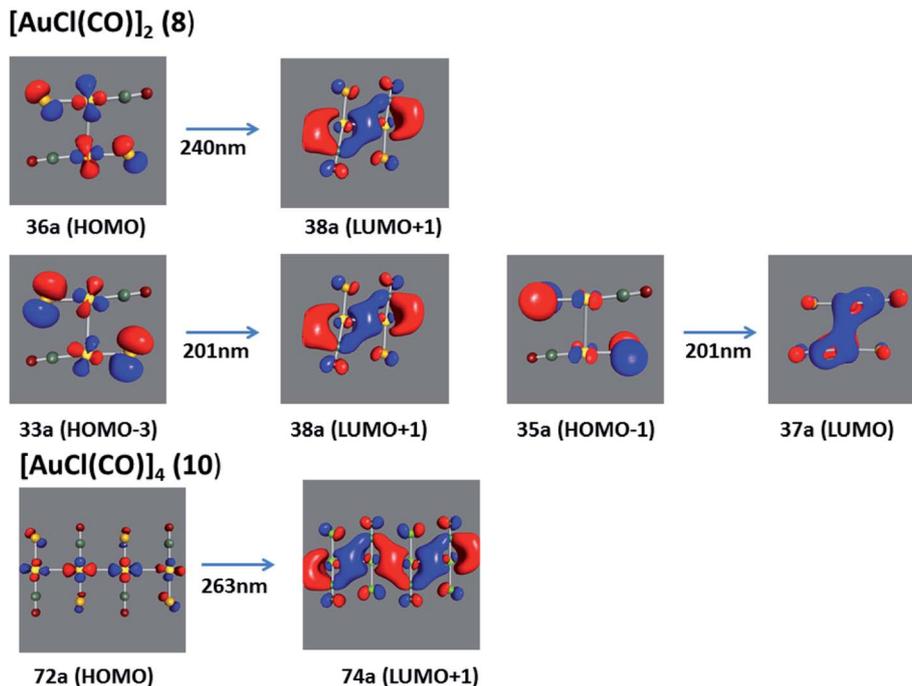
Table 8 Transition energies (in eV) and wavelengths (in nm) for the $S_0 \rightarrow S_1$ and $S_0 \rightarrow T_1$ absorption processes and for the $T_1 \rightarrow S_0$ emission process in the monomers and dimers in the models

System	Method	$S_0 \rightarrow S_1$ eV (nm)	$T_1 \rightarrow S_0$ eV (nm)	Stokes shift $S_0 \rightarrow S_1 \cdots T_1 \rightarrow S_0$ eV	$S_0 \rightarrow T_1$ eV (nm)	Stokes shift $S_0 \rightarrow T_1 \rightarrow S_0$ eV
$[AuCl(CNH)]$ (**1**)	SCS-CC2	6.37(195)	1.46(848)	4.91	6.04(205)	4.58
	B3LYP	5.32(233)	1.50(825)	3.82	5.21(238)	3.71
	PBE	5.10(243)	1.73(714)	3.37	4.95(251)	3.22
$[AuCl(CNH)]_2$ (**5**)	SCS-CC2	5.25(236)	2.84(436)	2.41	4.75(263)	1.91
	B3LYP	4.86(255)	2.63(471)	2.23	4.81(256)	2.18
	PBE	4.48(277)	1.87(662)	2.99	4.41(280)	2.54
$[AuCl(CO)]$ (**4**)	SCS-CC2	6.25(198)	1.48(836)	4.77	5.94(209)	4.46
	B3LYP	5.15(241)	1.52(833)	3.63	5.00(248)	3.48
	PBE	4.92(252)	1.48(837)	3.44	4.85(255)	3.37
$[AuCl(CO)]_2$ (**8**)	SCS-CC2	5.52(225)	2.99(414)	2.52	5.57(222)	2.58
	B3LYP	4.82(257)	2.33(532)	2.49	4.78(259)	2.45
	PBE	3.96(313)	2.05(604)	1.91	4.21(294)	2.16

Table 9 Optimized Au–Au distance, R_e (pm), for the dimer models $[AuCl(CNH)]_2$ and $[AuCl(CO)]_2$ in the S_0, S_1 and T_1 states

Model	Method	Au–Au (S_0)	Au–Au (S_1)	Au–Au (T_1)
$[AuCl(CNH)]_2$	SCS-MP2	356.6	281.9	263.7
	B3LYP	350.8	269.5	267.7
	PBE	352.6	269.5	268.8
$[AuCl(CO)]_2$	SCS-MP2	356.9	290.7	297.2
	B3LYP	345.9	273.7	271.3
	PBE	347.1	273.2	272.2

dependence between the Au–Au intermolecular contacts in the T_1 state and the optical bands with a shift effect seen in the experimental solid state data.

Conflicts of interest

There are no conflicts to declare.

Acknowledgements

References

1 G. M. Whitesides and R. F. Ismagliov, *Science*, 1999, **284**, 89–92.

2 R. F. Ludlow and S. Otto, *Chem. Soc. Rev.*, 2008, **37**, 101–108.

3 *Thinking in Complexity*, ed. K. Mainzer, Spinger-Verlang, New York, 3rd edn, 1997.

4 E. Mattia and S. Otto, *Nat. Nanotechnol.*, 2015, **10**, 111–119.

5 B. Grzybowski, S. Otto and D. Philp, *Chem. Commun.*, 2014, **50**, 14924–14925.

6 O. Miljanic, *Chem*, 2017, **2**, 502–524.

7 *Non-covalent Interactions in Quantum Chemistry and Physics*, ed. A. Otero de la Roza and G. DiLabio, Elsevier, 2017.

8 J. F. Ayme and J.-M. Lehn, *Adv. Inorg. Chem.*, 2018, **71**, 3–78.

9 A. S. Mahadevi and G. N. Sastry, *Chem. Rev.*, 2016, **116**, 2775–2825.

10 P. Pyykkö, *Chem. Soc. Rev.*, 2008, **37**, 1967–1997.

11 V. W.-W. Yam, V. K.-M. Au and S. Y.-L. Leung, *Chem. Rev.*, 2015, **115**, 7589–7728.

12 E. R. T. Tiekink, *Coord. Chem. Rev.*, 2017, **345**, 209–228.

13 P. Pyykkö, *Chem. Rev.*, 1997, **97**, 597–636.

14 P. Pyykkö, N. Runeberg and F. Mendizabal, *Chem.–Eur. J.*, 1997, **3**, 1451–1457.

15 N. Runeberg, M. Schütz and H.-J. Werner, *J. Chem. Phys.*, 1999, **110**, 7210–7215.

16 P. Pyykkö, *Angew. Chem., Int. Ed.*, 2004, **43**, 4412–4456.

17 E. O'Grady and N. Kaltsoyannis, *Phys. Chem. Chem. Phys.*, 2004, **6**, 680–687.

18 K. M.-C. Wong, V. K.-M. Au and V. W.-W. Yam, in *Comprehensive Inorganic Chemistry II*, ed. J. Reedijk and K. Poeppelmeier, Elsevier, Oxford, UK, 2nd edn, 2013, pp. 59–130.

19 M.-C. Tang, A. K.-W. Chan, M.-Y. Chan and V. W.-W. Yam, *Top. Curr. Chem.*, 2016, **46**, 374–405.

20 J. M. López-de-Luzuriaga, M. Monge and M. E. Olmos, *Dalton Trans.*, 2017, **46**, 2046–2067.

21 R. Donamaría, M. C. Gimeno, V. Lippolis, J. M. López-de-Luzuriaga, M. Monge and M. E. Olmos, *Inorg. Chem.*, 2016, **55**, 11299–11310.

22 *Modern Supramolecular Gold Chemistry*, ed. A. Laguna, Wiley-VCH, Weinheim, 2008.

23 E. J. Fernández, J. M. López-de-Luzuriaga, M. Monge, M. Montiel, M. E. Olmos, J. Pérez, A. Laguna, F. Mendizabal, A. A. Mohamed and J. P. Fackler, *Inorg. Chem.*, 2004, **43**, 3573–3581.

24 V. W.-W. Yam, A. K.-W. Chan and E. Y.-H. Hong, *Nat. Rev. Chem.*, 2020, **10**, 528–541.

25 F. Caddeo, V. Fernaández-Moreira, M. Arca, A. Pintus, A. Laguna, V. Lippolis and M. C. Gimeno, *Dalton Trans.*, 2021, **50**, 9709–9718.

26 *Gold-Progress in Chemistry, Biochemistry and Technology*, ed. H. Schmidbaur, John Wiley & Sons, New York, 1999.

27 H. Schmidbaur and A. Schier, *Chem. Soc. Rev.*, 2008, **37**, 1931–1951.

28 J. P. Fackler, *Inorg. Chim. Acta*, 2015, **424**, 83–90.

29 J. Gil-Rubio and J. Vicente, *Chem.–Eur. J.*, 2018, **24**, 32–46.

30 G. Tárkányi, P. Király, G. Pálinkás and A. Deák, *Magn. Reson. Chem.*, 2007, **45**, 917–924.

31 A. Deák, T. Megyes, G. Tárkányi, P. Király, L. Biczók, G. Pálinkás and P. J. Stang, *J. Am. Chem. Soc.*, 2006, **128**, 12668–12670.

32 F. Mendizabal, S. Miranda-Rojas and L. Barrientos, *Int. J. Quantum Chem.*, 2019, **119**, e25675.

33 P. Pyykkö and F. Mendizabal, *Inorg. Chem.*, 1998, **37**, 3018–3025.

34 F. Mendizabal and P. Pyykkö, *Phys. Chem. Chem. Phys.*, 2004, **4**, 900–905.

35 J. Muñiz, C. Wang and P. Pyykkö, *Chem.–Eur. J.*, 2011, **17**, 368–377.

36 R.-F. Liu, C. A. Franzese, R. Malek, P. S. Zuchowski, J. G. Angyan, M. M. Szczesniak and G. Chalasinski, *J. Chem. Theory Comput.*, 2011, **7**, 2399–2407.

37 M. Andrejic and R. A. Mata, *Phys. Chem. Chem. Phys.*, 2013, **15**, 18115–18122.

38 F. Mendizabal, S. Miranda-Rojas and L. Barrientos, *Comput. Theor. Chem.*, 2015, **1057**, 74–79.

39 E. Andris, P. C. Andrikopoulos, J. Schulz, J. Turek, A. Ruzicka, J. Roithova and L. Rulisek, *J. Am. Chem. Soc.*, 2018, **140**, 2316–2325.

40 F. Mendizabal, S. Miranda-Rojas and P. Castro-Latorre, *Mol. Simul.*, 2020, **46**, 521–529.

41 F. Mendizabal and S. Miranda-Rojas, *RSC Adv.*, 2020, **10**, 33549–33557.

42 P. Castro-Latorre, S. Miranda-Rojas and F. Mendizabal, *RSC Adv.*, 2020, **10**, 3895–3901.

43 L. Magnko, M. Schweizer, G. Rauhut, M. Schütz, H. Stoll and H.-J. Werner, *Phys. Chem. Chem. Phys.*, 2002, **4**, 1006–1013.

44 P. Pyykkö, X.-G. Xiong and J. Li, *Faraday Discuss.*, 2011, **152**, 169–178.

45 Q. Wan, J. Yang, W.-P. To and C.-M. Che, *Proc. Natl. Acad. Sci. U. S. A.*, 2021, **118**, e2019265118.

46 Q. Zheng, S. Borsley, G. S. Nichol, F. Duarte and S. L. Cockroft, *Angew. Chem., Int. Ed.*, 2019, **131**, 2–6.

47 M. B. Brands, J. Nitsch and C. Fonseca-Guerra, *Inorg. Chem.*, 2018, **57**, 2603–2608.

48 P. Pyykkö and F. Mendizabal, *Chem.–Eur. J.*, 1997, **3**, 1458–1465.

49 F. Mendizabal, *Organometallics*, 2001, **20**, 261–265.

50 R. L. White-Morris, M. M. Olmstead, A. L. Balch, O. Elbjeirami and M. A. Omary, *Inorg. Chem.*, 2003, **42**, 6741–6748.

51 H. Kunkely and A. Vogler, *J. Organomet. Chem.*, 1997, **541**, 177–179.

52 P. G. Jones, *Z. Naturforsch.*, 1982, **37b**, 823–824.

53 J. Perdew, K. Burke and M. Ernzerhof, *Phys. Rev. Lett.*, 1996, **77**, 3865–3869.

54 A. D. Becke, *Phys. Rev. A: At., Mol., Opt. Phys.*, 1988, **38**, 3098–3100.

55 A. D. Becke, *J. Chem. Phys.*, 2014, **140**, 18A301.

56 Y. Zhao and D. G. Truhlar, *J. Chem. Phys.*, 2006, **125**, 194101–194118.

57 S. Grimme, S. Ehrlich and H. Krieg, *J. Chem. Phys.*, 2010, **132**, 154104–154119.

58 W. Hujo and S. Grimme, *J. Chem. Theory Comput.*, 2011, **7**, 3866–3871.

59 S. F. Boys and F. Bernardi, *Mol. Phys.*, 1970, **19**, 553–566.

60 P. Habza and R. Zahradnik, *Chem. Rev.*, 1988, **88**, 871–897.

61 Turbomole: R. Ahlrichs, M. Bär, M. Häser, H. Horn and C. Kölmel, *Chem. Phys. Lett.*, 1989, **162**, 165–169.

62 M. J. Frisch, *et al.*, *Gaussian 16*, Pittsburgh, PA, 2003.

63 D. Andrae, M. Häusserman, H. Dolg, H. Stoll and H. Preuss, *Theor. Chim. Acta*, 1990, **77**, 123–141.

64 A. Bergner, M. Dolg, M. W. Küchle, H. Stoll and H. Preuss, *Mol. Phys.*, 1993, **80**, 1431–1443.

65 T. Dunning and P. Hay, in *Modern Theoretical Chemistry*, ed. H. Schaefer, Plenum Press, 1997, vol. 3, pp. 1–28.

66 R. Bauernschmitt and R. Ahlrichs, *Chem. Phys. Lett.*, 1996, **256**, 454–464.

67 L. Olsen and P. Jörgensen, in *Modern Electronic Structure Theory*, ed. D. R. Yarkony, World Scientific, River Edge, NJ, 1995, vol. 2.

68 N. O. Winter and C. Hättig, *J. Chem. Phys.*, 2011, **134**, 184101–184115.

69 M. Gerenkamp and S. Grimme, *Chem. Phys. Lett.*, 2004, **392**, 229–235.

70 N. O. Winter and C. Hättig, *Chem. Phys.*, 2012, **401**, 217–227.

71 H. Rabaa, M. A. Omary, S. Taubert and D. Sundholm, *Inorg. Chem.*, 2018, **57**, 718–730.

72 D. J. Liptropt and P. P. Power, *Nat. Rev. Chem.*, 2017, **1**, 004, DOI: 10.1038/s41570-016-0004.

73 A. D. Buckingham, P. W. Fowler and J. M. Hutson, *Chem. Rev.*, 1988, **88**, 963–988.

74 *The Theory of Intermolecular Forces*, ed. A. J. Stone, Clarendon Press, Oxford, 1996.

75 T. A. Koopmans, *Physica*, 1934, **1**(1–6), 104–113.